Electronic Supporting Information

Pure separation of acetylene based on a sulfonic acid and amino group functionalized Zn-MOF

Yu-Xin Deng, Guo-Ping Yang*, and Yao-Yu Wang*

Key Laboratory of Synthetic and Natural Functional Molecule of the Ministry of Education, Shaanxi Key Laboratory of Physico-Inorganic Chemistry, Xi'an Key Laboratory of Functional Supramolecular Structure and Materials, College of Chemistry & Materials Science, Northwest University, Xi'an 710127, Shaanxi, P. R. China.

**E-mail: ygp@nwu.edu.cn; wyaoyu@nwu.edu.cn.*

1. Materials and general methods

All solvents for synthesis were purchased commercially. Fourier transform infrared spectrum (FT-IR) was measured with a Nicolet FT-IR 170 SX spectrophotometer in the range 4000-400 cm^{-1}. Powder X-ray diffraction (PXRD) pattern was recorded on a Bruker D8 ADVANCE X-ray powder diffractometer (Cu Kα, 1.5418 Å). Thermalgravimetric analyses (TGA) were carried out in a nitrogen stream using a Netzsch TG209F3 equipment at a heating rate of 10 °C min^{-1}. Single crystal diffraction data were collected on a Bruker SMART APEX II CCD single crystal diffractometer. Gas adsorption measurements were performed with an automatic volumetric sorption apparatus (Micrometrics ASAP 2020M). Breakthrough experiments were performed on a Quantachrome dynaSorb BT equipment.

1.1 Synthesis of $[Zn_3(SNDC)(AmTAZ)_3(H_2O)]\cdot H_2O\cdot CH_3CN$ (1).

$Zn(NO_3)_2\cdot 6H_2O$ (0.029 g, 0.1 mmol), H_3SNDC (0.015 g, 0.05 mmol), AmTAZ (0.004 g, 0.05 mmol), CH_3CN (3 mL), H_2O (3 mL) and two drops of alkali solution (1 M NaOH) were added to a glass vial with stirring to dissolve the mixture. The solution was then transferred to an oven set at 105 °C. After heating for 72 h and following a cooling procedure, light yellow transparent block crystals of **1** were obtained (yield: 78%). FT-IR (KBr, cm^{-1}) (Fig. S4): 3420 (s), 1620 (s), 1370 (m), 1340 (m), 1210 (m), 1120 (w), 1040 (w), 828 (w), 760 (w), 677 (w), 572 (w), 486 (w).

2. X-Ray Crystallography

The single-crystal Xray diffractions were tested on Bruker SMART APEX II CCD diffractometer equipped with graphite monochromated Mo Kα radiation (λ = 0.71073 Å) *via* ϕ/ω scan method. The diffraction data were corrected for Lorentz and polarization effects for empirical absorption based on multiscan. The structures were solved by the direct methods and refined on F^2 via *SHELXTL* program. The anisotropic thermal parameters were applied to non-hydrogen atoms. The hydrogen atoms of ligands were calculated and added at ideal positions. The crystallographic data of **1** and **1a** are summarized in Table S2, and the selected bond lengths and angles are listed in Table S3, S4. The disordered lattice molecules were refined by the SQUEEZE program and this result is consistent to the results of TGA.

In **1**, the Zn1 centre was accomplished by one O atom from carboxylic acid group on SNDC and three N atoms from three distinct AmTAZ. Zn2 centre was formed by one O atom from sulfonic acid group on SNDC and three N atoms from three different AmTAZ. Zn3 centre was

formed by one O atom from a carboxylate of SNDC, one O atom on the axial position originating from water and three N atoms from ligand AmTAZ. In **1a**, the Zn1 centre was accomplished by one O atom from carboxylic acid group on SNDC and three N atoms from three distinct AmTAZ. Zn2 centre was formed by one O atom from sulfonic acid group on SNDC and three N atoms from three different AmTAZ. Zn3 was formed with one O coming from the carboxylic acid group of SNDC and three N atoms coming from the ligand AmTAZ.

3. Gas Sorption Experiments

Before the gas adsorption experiment, the synthesized samples were activated at 473 K vacuum for 4 h. Gas adsorption measurements were then performed using the Micrometrics ASAP 2020M gas Adsorption Analyzer.

3.1 Fitting Adsorption Heat of Pure Component Isotherms

The adsorbate molecules (C_2H_2, CO_2 and CH_4) and the adsorbent lattice atoms is reflected in the isosteric heat of adsorption (Q_{st}) using Virial 2 model, which define as:

$$lnP = lnN + 1/T \sum_{i=0}^{m} a_i N^i + \sum_{i=0}^{n} b_i N^i \quad (1)$$

$$Q_{\mathrm{st}} = -R \sum_{i=0}^{m} a_i N^i \quad (2)$$

Here, Q_{st} is the coverage-dependent enthalpy of adsorption, P is the pressure (mmHg), N is the adsorbed amount (mg/g), T is the temperature (K), a_i and b_i are virial coefficients, and m and n represent the number of coefficients used to describe the isotherms. Q_{st} is the coverage-dependent enthalpy of adsorption and R is the universal gas constant. A virial-type equation (**1**) was used to fit adsorption data at 273 K and 298 K, and then the values of a_0 through a_m were used to calculate the isosteric heat of adsorption using equation (**2**).

3.2 Ideal Adsorbed Solution Theory (IAST)

The experimental measured loadings for pure C_2H_2, CO_2 and CH_4 (measured at 273 and 298 K) in samples were fitted with a Langmuir-Freundlich (L-F) model (equation **3**):

$$q = \frac{a_1 * b_1 * p^{c_1}}{1 + b_1 * p^{c_1}} \quad (3)$$

Where q and p are adsorbed amounts per mass of adsorbent (mmol/g) and pressures of component i (kPa), respectively.

IAST calculations of adsorption selectivity for binary mixtures defined by equation **4**:

$$S_{i/j} = \frac{x_i * y_i}{x_j * y_i} \quad (4)$$

Where x_i and x_j are the molar loadings in the adsorbed phase in equilibrium with the bulk gas phase with partial pressures y_i, and y_j. We calculate the values of x_i and x_j using IAST of Myers and Prausnitz.

3.3 Dynamic Gas Breakthrough Experiments

The as-synthesized sample 0.966 g of **1a** (966 mg) was degasified in-situ in the column through vacuuming at 473 K for 4 h before the measurement. The breakthrough experiment was performed on the Quantachrome dynaSorb BT equipments at 298 K and 1 bar with an equal volume of mixed gas (gas A: gas B: Ar = 5%: 5%: 90% or gas A: gas B: gas C: Ar = 5%: 5%: 5%: 85%, Ar as the carrier gas, flow rate = 6 mL min^{-1}). The activated **1a** was filled into a packed column of ϕ 4.2×80 mm, and then the packed column was washed with Ar at a rate of 6 mL min^{-1} at 343 K for 60 minutes to further activate the samples. Between two breakthrough experiments, the adsorbent was regenerated by Ar flow of 6 mL min^{-1} for 35 min at 353 K to guarantee a complete removal of the adsorbed gases. The outlet composition was continuously monitored by gas chromatograph until complete breakthrough was achieved. On the basis of the gas balance, the gas adsorption capacities can be determined as follows:

$$q_i = \frac{C_i V}{22.4 \times m} \times \int_0^t \left(1 - \frac{F}{F_0}\right) dt \quad (5)$$

Where q_i is the equilibrium adsorption capacity of gas i (mmol/g), C_i is the feed gas concentration, V is the volumetric feed flow rate (cm^3/min), t is the adsorption time (min), F_0 and F are the inlet and outlet gas molar flow rates, respectively, and m is the mass of the adsorbent (g).

The separation factor (α) of the breakthrough experiment is determined as:

$$\alpha = \frac{q_1 y_2}{q_2 y_1} \quad (6)$$

In which y_i is the molar fraction of gas i in the gas mixture.

3.4 Grand canonical Monte Carlo (GCMC) simulations

All simulations were performed by the Materials Studio (MS) 2020 package.

The preferred sorption locations were performed by GCMC simulations with Adsorption fixed loading task and Metropolis method[1] in the sorption calculation module. As for all of the

GCMC simulations, the framework was considered to be rigid. The framework and gas molecule were described by the forcefiled of universal force field (UFF). The cutoff radius was set to 12.5 Å, for the Lennard-Jones (LJ) interactions, and the electrostatic interactions, and the Ewald summation method was selected to calculate the electrostatic interactions between adsorbates as well as between adsorbates and the framework. For state point in GCMC simulation, the system adopted 1×10^6 Monte Carlo steps to guarantee equilibration, and the ultimate data was collected for another 1×10^7 Monte Carlo steps. The charges of the atoms of both gas molecules and the framework were assigned by QEq method.

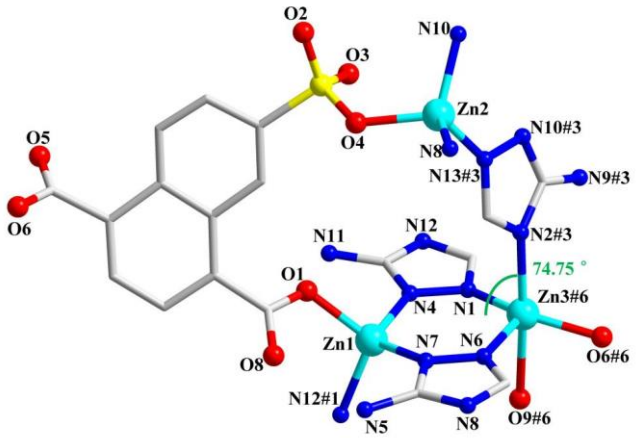

Fig. S1 Coordination environment of Zn^{2+} ions in **1** (Symmetric code: #1 -x, y+1/2, -z+1/2; #2 -x, -y+1, -z+1; #3 -x, -y, -z+1; #4 x+1, y, z; #5 -x+1, -y, -z+1; #6 x-1, y, z; #7 -x, y-1/2, -z+1/2).

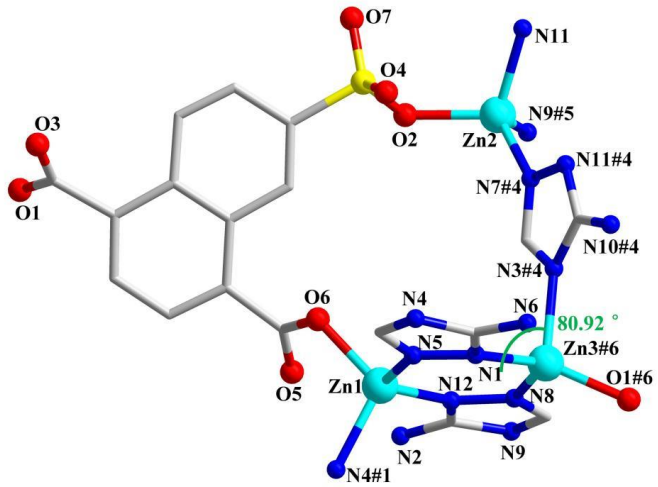

Fig. S2 Coordination environment of Zn^{2+} ions in **1a** (Symmetric code: #1 -x+2, y-1/2, -z+3/2; #2 x-1, y, z; #3 -x+1, -y+1, -z+1; #4 -x+2, -y+1, -z+1; #5 -x+2, -y, -z+1; #6 x+1, y, z; #7 -x+2, y+1/2, -z+3/2).

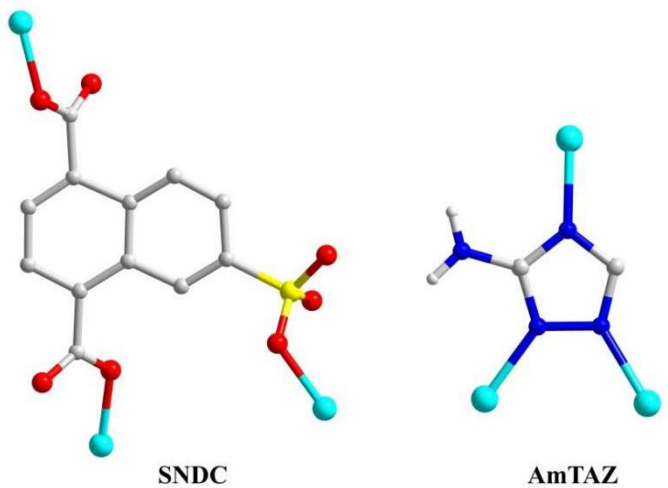

Fig. S3 Coordination modes of SNDC and ancillary ligand AmTAZ in **1**.

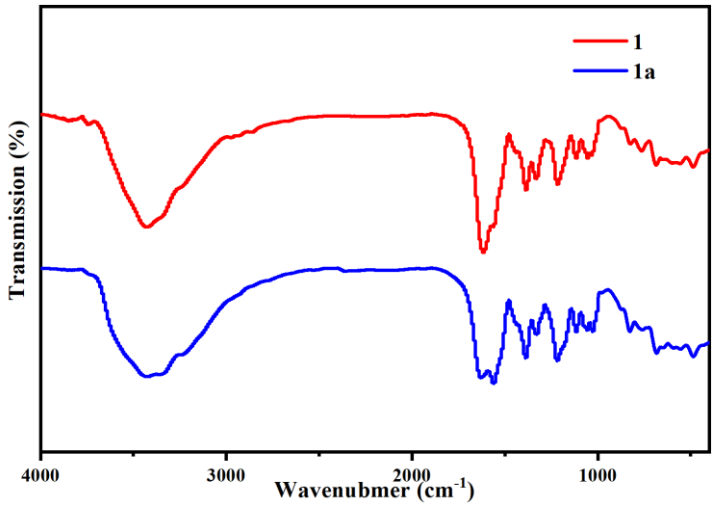

Fig. S4 FT-IR spectra of complexes **1** and **1a**.

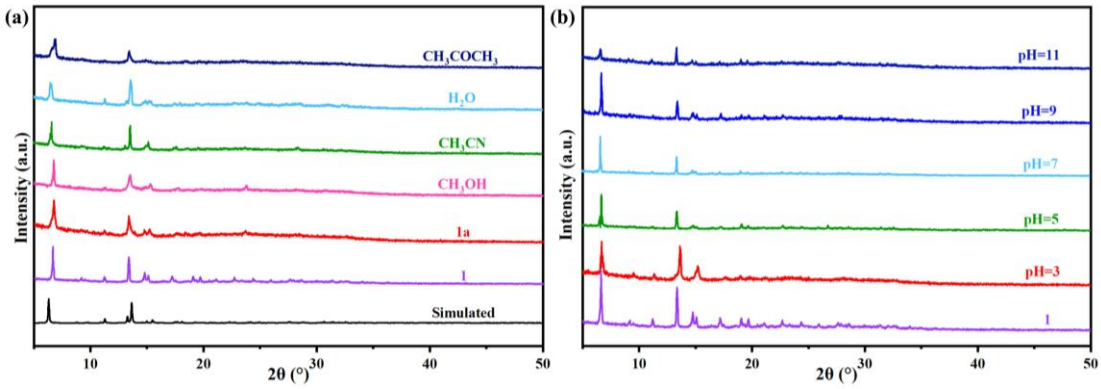

Fig. S5 PXRD patterns of (a) simulated **1**, as-synthesized **1**, tested **1a**, **1** in different solvents for 12 h and (b) **1** in aqueous solutions of different pH for 12 h.

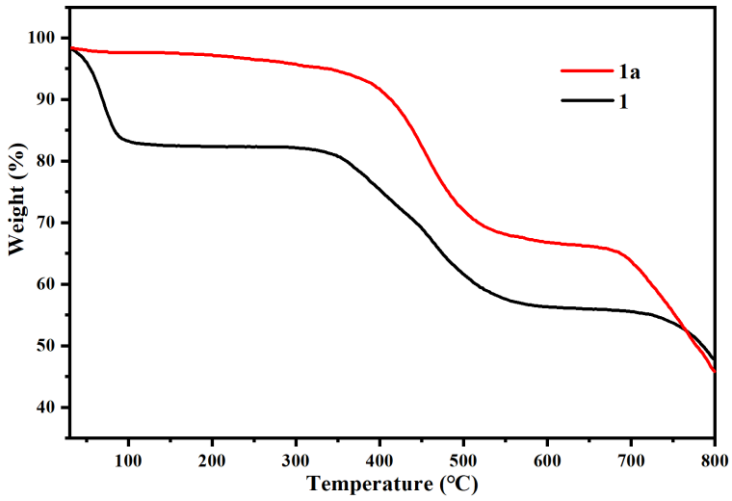

Fig. S6 TGA curve of as-synthesized **1** and adsorbent **1a**

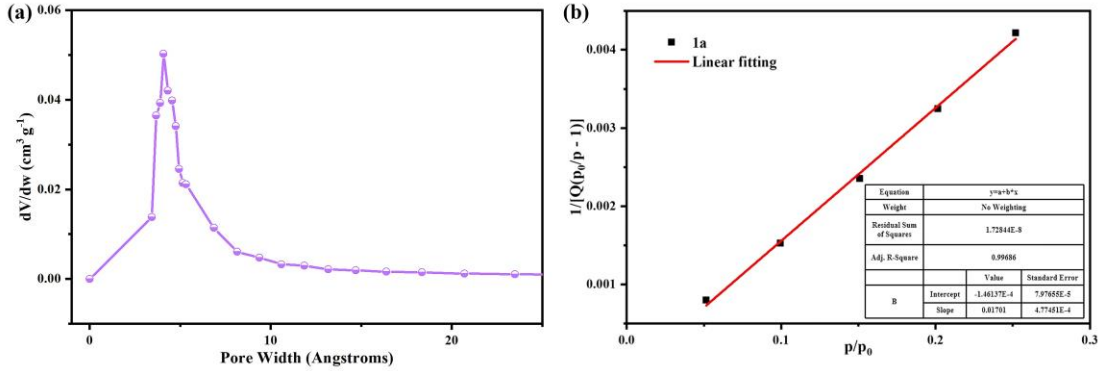

Fig. S7 (a) The pore size distribution of **1a** (mainly at 4.0 Å), as calculated by Original Density Functional Theory. (b) The BET surface area plot for **1a**.

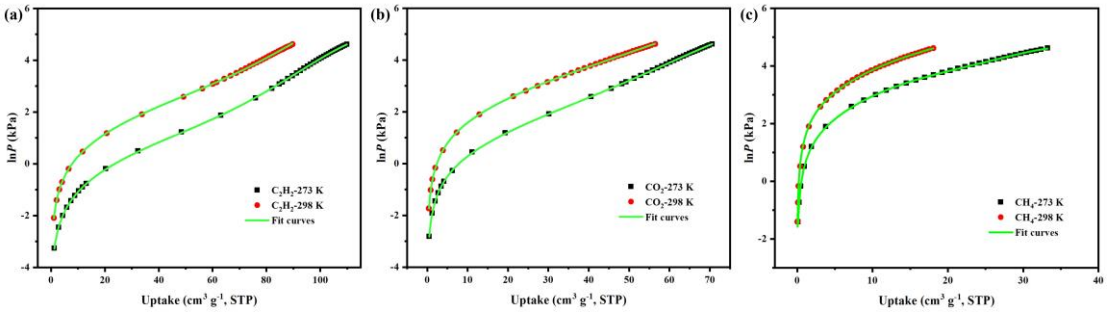

Fig. S8 Virial fitting of (a) C_2H_2, (b) CO_2 and (c) CH_4 adsorption isotherms (points) for Q_{st} calculation on **1a**.

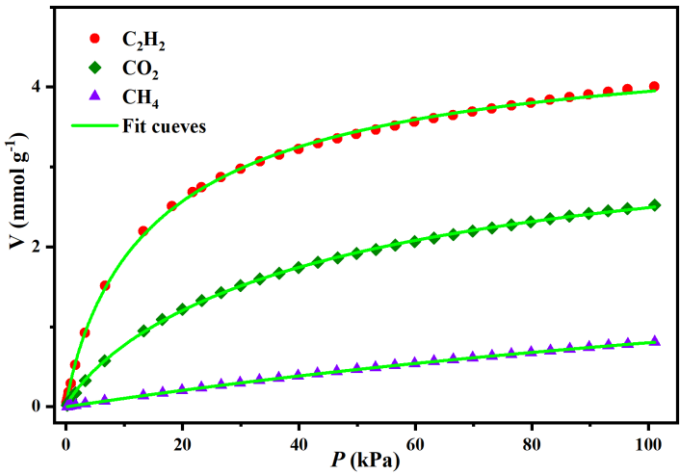

Fig. S9 Single-site Langmuir-Freundlich fitting of C_2H_2, CO_2 and CH_4 adsorption isotherms on **1a** at 298 K.

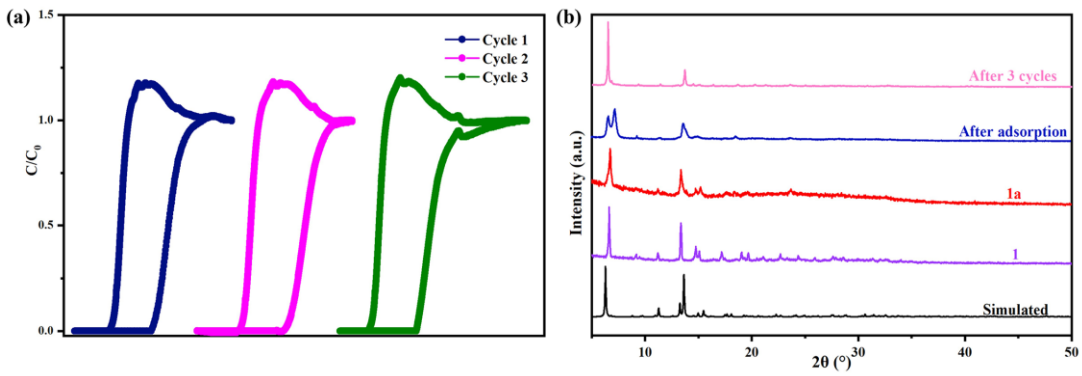

Fig. S10 (a) Three cycles of breakthrough experiment for the equimolar C_2H_2/CO_2 in **1a**. (b) PXRD patterns showing the stability of **1a**.

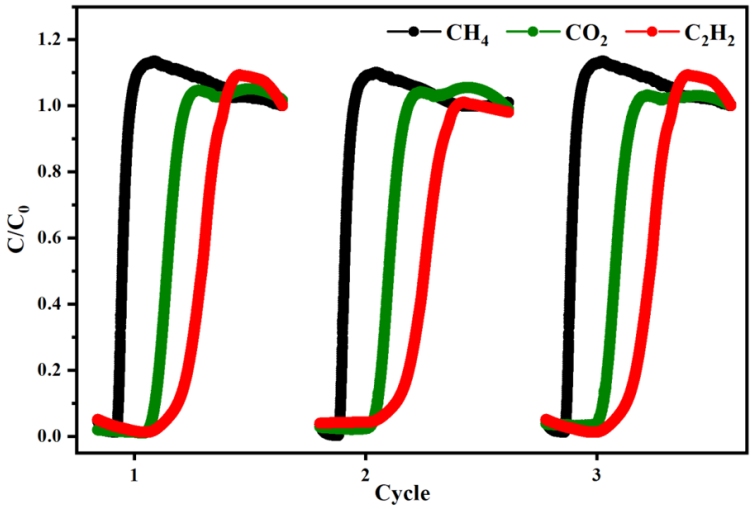

Fig. S11 Three cycles of breakthrough experiment for the equimolar $C_2H_2/CO_2/CH_4$ in **1a**.

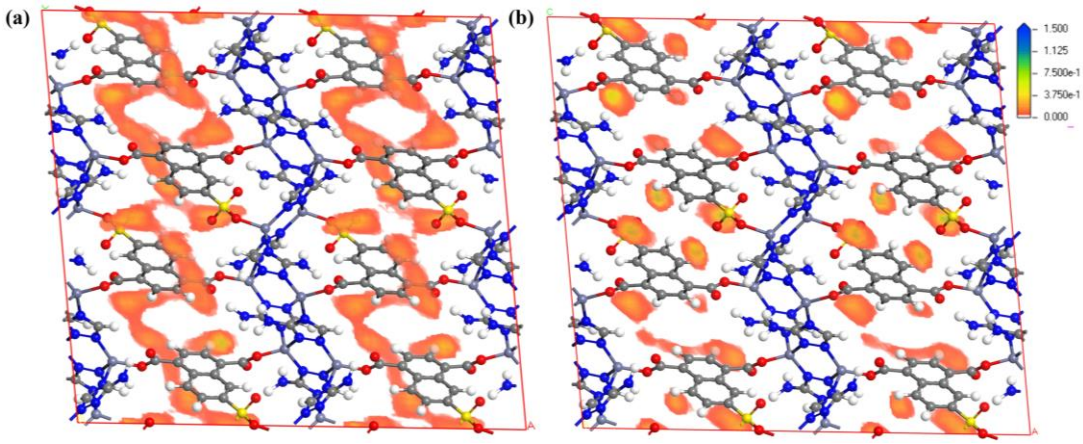

Fig. S12 Simulated probability density distribution profile of C_2H_2 (a) and CO_2 (b) in **1a** by GCMC simulation at 100 kPa and 298 K. (Note: C_2H_2 was more concentrated in the voids of the adsorbent than CO_2, which was compatible with experimental results.).

Table S1. Physicochemical characteristics of different gases

	Boiling point (K)	Molecular dimensions (Å)	Polarizability (Å^3)	Quadrupole moment×10^{26}/esu cm^2
C_2H_2	189.3	3.32×3.34×5.7	3.33-3.93	7.5
CO_2	194.7	3.18×3.33×5.36	2.91	-4.3
CH_4	111.66	3.82×3.94×4.10	2.59	0

Table S2. Crystallographic data of **1** and **1a**.

Compond	1	1a
Empirical formula	$C_{20}H_{21}N_{13}O_9SZn_3$	$C_{18}H_{14}N_{12}O_7SZn_3$
Formula mass	815.60	738.58
Crystal system	Monoclinic	Monoclinic
Space group	$P2_1/c$	$P2_1/c$
a [Å]	14.143(2)	14.0795(7)
b [Å]	9.9829(15)	9.8510(5)
c [Å]	25.111(5)	25.9541(12)
α [Å]	90	90
β [Å]	96.777(5)	95.909(2)
γ [Å]	90	90
V [Å^3]	3520.6(10)	3580.6(3)
Z	4	4
$D_{calcd.}$ [Mg·m^{-3}]	1.427	1.370
F(000)	1512	1472
R_{int}	0.0508	0.0425
GOF on F^2	1.029	1.054
R_1^a, wR_2^b [I > 2σ]	R_1 = 0.0896, wR_2 = 0.2568	R_1 = 0.0537, wR_2 = 0.1716
R_1^a, wR_2^b (all data)	R_1 = 0.1191, wR_2 = 0.2797	R_1 = 0.0636, wR_2 = 0.1802

$^aR_1 = \Sigma(|F_0| - |F_c|)/\Sigma|F_0|$. $^bwR_2 = [\Sigma w(F_0^2 - F_c^2)^2 / \Sigma w(F_0^2)^2]^{1/2}$

Table S3. Selected bond lengths [Å] and angles [°] for **1**.

Compound 1			
Zn(1)-O(1)	1.950(7)	N(1)#4-Zn(3)-O(9)	80.5(4)
Zn(1)-N(4)	1.986(8)	N(1)#4-Zn(3)-N(2)#5	91.5(3)
Zn(1)-N(7)	1.982(8)	N(1)#4-Zn(3)-N(6)#4	111.7(3)
Zn(1)-N(12)#1	2.010(8)	N(2)#5-Zn(3)-O(9)	171.6(4)
Zn(2)-O(4)	1.954(7)	N(6)#4-Zn(3)-O(9)	88.8(4)
Zn(2)-N(8)#2	1.994(8)	N(6)#4-Zn(3)-N(2)#5	96.8(3)
Zn(2)-N(10)	1.968(8)	C(3)-O(1)-Zn(1)	120.0(8)
Zn(2)-N(13)#3	1.985(8)	S(1)-O(4)-Zn(2)	124.9(5)
Zn(3)-O(6)	1.941(8)	C(18)-O(6)-Zn(3)	116.1(9)
Zn(3)-O(9)	2.368(10)	Zn(3)-O(9)-H(9A)	109.2
Zn(3)-N(1)#4	1.999(7)	Zn(3)-O(9)-H(9B)	109.4
Zn(3)-N(2)#5	2.120(9)	N(4)-N(1)-Zn(3)#6	120.6(6)
Zn(3)-N(6)#4	2.013(8)	C(1)-N(1)-Zn(3)#6	132.4(6)
O(1)-Zn(1)-N(4)	100.2(3)	C(1)-N(1)-N(4)	105.5(7)
O(1)-Zn(1)-N(7)	120.1(4)	C(4)-N(2)-Zn(3)#5	126.1(7)
O(1)-Zn(1)-N(12)#1	107.3(3)	C(6)-N(2)-Zn(3)#5	131.1(8)
N(4)-Zn(1)-N(12)#1	114.2(4)	N(1)-N(4)-Zn(1)	126.1(6)
N(7)-Zn(1)-N(4)	111.0(3)	C(12)-N(4)-Zn(1)	127.9(7)
N(7)-Zn(1)-N(12)#1	104.4(3)	C(12)-N(4)-N(1)	105.8(8)
O(4)-Zn(2)-N(8)#2	102.0(3)	N(7)-N(6)-Zn(3)#6	124.8(6)
O(4)-Zn(2)-N(10)	108.7(4)	C(10)-N(6)-Zn(3)#6	130.2(6)
O(4)-Zn(2)-N(13)#3	114.0(4)	C(10)-N(6)-N(7)	105.0(8)
N(10)-Zn(2)-N(8)#2	112.7(4)	N(6)-N(7)-Zn(1)	122.6(6)
N(10)-Zn(2)-N(13)#3	110.8(3)	C(8)-N(7)-Zn(1)	130.5(7)
N(13)#3-Zn(2)-N(8)#2	108.6(4)	C(8)-N(8)-Zn(2)#2	128.0(7)
O(6)-Zn(3)-N(1)#4	143.3(4)	C(10)-N(8)-Zn(2)#2	128.6(7)
O(6)-Zn(3)-N(2)#5	101.1(4)	N(13)-N(10)-Zn(2)	122.9(6)
O(6)-Zn(3)-N(6)#4	101.0(4)	C(6)-N(10)-Zn(2)	131.5(6)
C(1)-N(12)-Zn(1)#7	125.6(7)	N(10)-N(13)-Zn(2)#3	126.1(6)
C(12)-N(12)-Zn(1)#7	129.4(7)	C(4)-N(13)-Zn(2)#3	129.2(7)

Symmetric code: #1 -x, y+1/2, -z+1/2; #2 -x, -y+1, -z+1; #3 -x, -y, -z+1; #4 x+1, y, z; #5 -x+1, -y, -z+1; #6 x-1, y, z; #7 -x, y-1/2, -z+1/2.

Table S4. Selected bond lengths [Å] and angles [°] for **1a**.

Compound 1a			
Zn(1)-O(4)	1.955(3)	O(6)-Zn(3)-N(13)	107.54(18)
Zn(1)-N(2)#1	2.006(4)	N(8)#4-Zn(3)-N(10)#5	110.79(17)
Zn(1)-N(6)	1.976(4)	N(8)#4-Zn(3)-N(13)	110.26(17)
Zn(1)-N(12)	2.009(4)	N(10)#5-Zn(3)-N(13)	111.07(17)
Zn(2)-O(1)	1.917(4)	C(18)-O(1)-Zn(2)	116.9(4)
Zn(2)-N(1)#2	1.986(4)	C(20)-O(4)-Zn(1)	115.1(4)
Zn(2)-N(4)#2	2.001(4)	S(1)-O(6)-Zn(3)	121.2(2)
Zn(2)-N(7)#3	2.064(4)	N(12)-N(1)-Zn(2)#6	120.3(3)
Zn(3)-O(6)	1.968(4)	C(1)-N(1)-Zn(2)#6	131.3(3)
Zn(3)-N(8)#4	1.975(4)	C(1)-N(2)-Zn(1)#7	128.6(4)
Zn(3)-N(10)#5	1.983(4)	C(13)-N(2)-Zn(1)#7	127.2(3)
Zn(3)-N(13)	1.986(4)	N(6)-N(4)-Zn(2)#6	125.2(3)
O(4)-Zn(1)-N(2)#1	109.51(17)	C(6)-N(4)-Zn(2)#6	128.2(3)
O(4)-Zn(1)-N(6)	120.66(17)	N(4)-N(6)-Zn(1)	123.1(3)
O(4)-Zn(1)-N(12)	99.79(16)	C(4)-N(6)-Zn(1)	130.4(3)
N(2)#1-Zn(1)-N(12)	112.55(18)	C(8)-N(7)-Zn(2)#3	131.3(3)
N(6)-Zn(1)-N(2)#1	104.66(16)	C(12)-N(7)-Zn(2)#3	125.0(3)
N(6)-Zn(1)-N(12)	109.87(15)	C(12)-N(7)-C(8)	102.9(4)
O(1)-Zn(2)-N(1)#2	135.61(18)	N(13)-N(8)-Zn(3)#4	124.2(3)
O(1)-Zn(2)-N(4)#2	99.32(18)	C(12)-N(8)-Zn(3)#4	130.2(3)
O(1)-Zn(2)-N(7)#3	108.24(18)	C(4)-N(10)-Zn(3)#5	128.3(3)
N(1)#2-Zn(2)-N(4)#2	111.01(15)	C(6)-N(10)-Zn(3)#5	127.5(3)
N(1)#2-Zn(2)-N(7)#3	97.39(16)	N(1)-N(12)-Zn(1)	127.3(3)
N(4)#2-Zn(2)-N(7)#3	100.68(16)	C(13)-N(12)-Zn(1)	126.2(3)
O(6)-Zn(3)-N(8)#4	114.95(19)	N(8)-N(13)-Zn(3)	125.5(3)
O(6)-Zn(3)-N(10)#5	101.94(17)	C(8)-N(13)-Zn(3)	128.2(3)

Symmetric code: #1 -x+2, y-1/2, -z+3/2; #2 x-1, y, z; #3 -x+1, -y+1, -z+1; #4 -x+2, -y+1, -z+1; #5 -x+2, -y, -z+1; #6 x+1, y, z; #7 -x+2, y+1/2, -z+3/2.

Table S5. Comparison of C_2H_2 uptake amount and Q_{st} of some MOF adsorbents for C_2H_2/CO_2 and C_2H_2/CH_4 separation at 1 bar

MOFs	**C_2H_2 uptake**	**C_2H_2 Q_{st}**	**Gas selectivity**		**Ref.**
	(cm^3 g^{-1})	**(kJ mol^{-1})**	**C_2H_2/CO_2**	**C_2H_2/CH_4**	
$Cu_{0.5}(tztp)_{0.5}$	135.0	38.3	2.7	23	2
Zn-MOF-74	122	43.8	3	--	3
$Ca(dtztp)_{0.5}$	110.0	28.9	1.7	33.3	4
FJU-89a	101.4	31.0	4.5	45.6	5
1a	**89.7**	**36.5**	**4.8**	**59.0**	**This work**
ZJU-74	85.7(296K)	45	36.5	1312.9	6
Ni(dpip)	83.6	41.7	2	18.5	7
ZJNU-133	81.8	30.7	3.1	15.4	8
ZJUT-2a	76	41.5	10	--	9
JCM-1	75	36.9	1.47	--	10
NbU-10	62.5(293 K)	31.3	2.8	--	11
BSF-1	52.6	31	3.3	46.9	12
FJU-36a	52.2(296 K)	32.9	2.8	17.7	13
TCuCl	49.3	41	5.3	--	14
DICRO-4-Ni-i	43	37.7	13.9	--	15
SNNU-17	37.8	30.5	1.2	20.3	16
JNU-1	27.4	13	3.6	--	17
M'MOF-2a	--	37.7	1.89	--	18

Table S6. Fitting parameters of the adsorption heats for **1a**.

Model	**Q_{st} (User)**		
Equation	y = ln(x)+1/K*(a0+a1*x+a2*x^2+a3*x^3+a4*x^4+a5*x^5)+(b0+b1*x+b2*x^2)		
Plot	C_2H_2-298K	CO_2-298K	CH_4-298K
a0	-4380.41933	-4082.07266	-3086.33286
a1	-8.7023	-22.0224	11.12365
a2	0.23975	0.84978	1.68475
a3	-0.0044	-0.00858	-0.20562
a4	$5.83271*10^{-5}$	$1.39829*10^{-4}$	0.00624
a5	$-2.42837*10^{-7}$	$-8.12035*10^{-7}$	$-6.87322*10^{-5}$
b0	12.54134	12.79701	11.90174
b1	0.03866	0.08479	-0.09053
b2	$-2.86216*10^{-4}$	-0.00195	0.00481
Reduced Chi-Sqr	$1.62282*10^{-4}$	$1.01849*10^{-4}$	0.0013
R-Square (COD)	0.99997	0.99998	0.99991
Adj. R-Square	0.99997	0.99997	0.99949

Table S7. Fitting parameters of the selectivity for **1a**.

Model	**LF (User)**		
Equation	a1*b1*x^c1/(1+b1*x^c1)		
Plot	C_2H_2-298K	CO_2-298K	CH_4-298K
a1	4.78219±0.0478	3.86608±0.06723	2.68996±0.03204
b1	0.08573±0.00223	$0.03412±6.81218*10^{-4}$	$0.00394±2.04387*10^{-5}$
c1	0.87027±0.01411	0.86269±0.01262	1.01594±0.00282
Reduced Chi-Sqr	$7.97619*10^{-4}$	$1.64982*10^{-4}$	$4.2004*10^{-7}$
R-Square (COD)	0.99958	0.99977	0.99999
Adj. R-Square	0.99956	0.99976	0.99999

Table S8. The simulation result summary for **1a** adsorbing C_2H_2 and CO_2.

Gas	**Calculated Q_{st} (kJ mol^{-1})**	**Experimental Q_{st} (kJ mol^{-1})[a]**
C_2H_2	36.7	36.5
CO_2	36.2	34.0

[a]Heat of adsorption at zero coverage.

Reference

[1] N. Metropolis, A.W. Rosenbluth, M.N. Rosenbluth, A.H. Teller, E. Teller. *J. Chem. Phys.,* 1953, **21**, 1087-1092.

[2] X. Y. Li, Y. Z. Li, L. N. Ma, L. Hou, C. Z. He, Y. Y. Wang, and Z. Zhu. *J. Mater. Chem. A,* 2020, **8**, 5227-5233.

[3] F. Luo, C. Yan, L. Dang, R. Krishna, W. Zhou, H. Wu, X. Dong, Y. Han, T. L. Hu, M. O'Keeffe, L. Wang, M. Luo, R. B. Lin, and B. Chen. *J. Am. Chem. Soc.,* 2016, **138**, 5678-5684.

[4] G. D. Wang, Y. Z. Li, W. F. Zhang, L. Hou, Y. Y. Wang, Z. Zhu. *ACS Appl. Mater. Interfaces,* 2021, **13**, 58862-58870.

[5] Y. X. Ye, S. M. Chen, L. J. Chen, J. T. Huang, Z. L. Ma, Z. Y. Li, Z. Z. Yao, J. D. Zhang, Z. J. Zhang, and S. C. Xiang. *ACS Appl. Mater. Interfaces,* 2018, **10**, 30912-30918.

[6] J. Pei, K. Shao, J. X. Wang, H. M. Wen, Y. Yang, Y. Cui, R. Krishna, B. Li, and G. A. Qian. *Adv. Mater.,* 2020, **32**, 1908275.

[7] Y. Z. Li, G. D. Wang, L. N. Ma, L. Hou, Y. Y. Wang, and Z. Zhu. *ACS Appl. Mater. Interfaces,* 2021, **13**, 4102-4109.

[8] L. Yue, X. Wang, R. Guo, Y. Lv, T. Zhang, B. Li, S. Lin, Y. Liang, D. L. Chen, and Y. He. *Inorg. Chem.,* 2023, **62**, 2415-2424.

[9] H. M. Wen, C. Liao, L. Li, L. Yang, J. Wang, L. Huang, B. Li, B. Chen, and J. Hu. *Chem. Commun.,* 2019, **55**, 11354-11357.

[10] G. D. Wang, H. H. Wang, W. J. Shi, L. Hou, Y. Y. Wang, and Z. Zhu. *J. Mater. Chem. A,* 2021, **9**, 24495-24502.

[11] J. Zhao, Q. Li, X. C. Zhu, J. Li, and D. Wu. *Inorg. Chem.,* 2020, **59**, 14424-14431.

[12] Y. Zhang, L. Yang, L. Wang, S. Duttwyler, and H. Xing. *Angew. Chem. Int. Ed.,* 2019, **58**, 8145-8150.

[13] L. Liu, Z. Yao, Y. Ye, L. Chen, Q. Lin, Y. Yang, Z. Zhang, and S. Xiang. *Inorg. Chem.,* 2018, **57**, 12961-12968.

[14] S. Mukherjee, Y. He, D. Franz, S. Q. Wang, W. R. Xian, A. A. Bezrukov, B. Space, Z. Xu, J. He, and M. J. Zaworotko. *Chem. Eur. J.,* 2020, **26**, 4923-4929.

[15] H. S. Scott, M. Shivanna, A. Bajpai, D. G. Madden, K. J. Chen, T. Pham, K. A. Forrest, A. Hogan, B. Space, J. J. Perry IV and M. J. Zaworotko. *ACS Appl. Mater. Interfaces,* 2017, **9**,

33395-33400.

[16] H. P. Li, Y. Y. Xue, Y. Wang, H. Sun, M. C. Hu, S. N. Li, Y. Jiang, and Q. G. Zhai. *Cryst. Growth Des.,* 2021, **21**, 1718-1726.

[17] H. Zeng, M. Xie, Y. L. Huang, Y. Zhao, X. J. Xie, J. P. Bai, M. Y. Wan, R. Krishna, W. Lu, and D. Li. *Angew. Chem. Int. Ed.,* 2019, **58**, 8515-8519.

[18] S. C. Xiang, Z. Zhang, C. G. Zhao, K. Hong, X. Zhao, D. R. Ding, M. H. Xie, C. D. Wu, M. C. Das, R. Gill, K. M. Thomas, and B. Chen. *Nat. Commun.,* 2011, **2**, 204.